Optical conductivity of graphene in the presence of random lattice deformations

Andreas Sinner, A. Sedrakyan, Klaus G. Ziegler

Optical conductivity of graphene in the presence of random lattice deformations

A. Sinner,[1] A. Sedrakyan,[1,2] and K. Ziegler[1]

[1]*Institute for Physics, Universität Augsburg, Universitätsstraße 1, D-86159 Augsburg, Germany*
[2]*Yerevan Physics Institute, Br. Alikhanian 2, Yerevan 36, Armenia*

We study the influence of lattice deformations on the optical conductivity of a two-dimensional electron gas. Lattice deformations are taken into account by introducing a non-Abelian gauge field into the Euclidean action of two-dimensional Dirac electrons. This is in analogy to the introduction of gravitation in four-dimensional quantum field theory. We examine the effect of these deformations on the averaged optical conductivity. Within the perturbative theory up to second order we show that corrections of the conductivity due to the deformations cancel each other exactly. We argue that these corrections vanish to any order in perturbative expansion.

I. INTRODUCTION

Graphene, a two-dimensional (2D) sheet of carbon atoms forming a honeycomb lattice, has outstanding electronic properties.[1–3] This is due to the fact that there are two bands that touch each other at two Dirac nodes. Moreover, the low-energy quasiparticles of undoped graphene experience a linear dispersion around two Dirac nodes. Transport properties, characterized by the longitudinal conductivity at the Dirac nodes, are quite robust and do not vary much from sample to sample. Exactly at the Dirac point a minimal conductivity has been observed in a number of experiments.[1,2,4] There are two important questions regarding this minimal conductivity: (i) is the value of the minimal conductivity "universal" (i.e., independent of additional modifications of the graphene sheet such as ripples or impurities) and (ii) what is its actual value in units of e^2/h? A discrepancy between the calculated conductivity of Dirac fermions and the experimentally observed minimal conductivity of graphene by a factor of roughly $1/\pi$ has been the subject of a substantial number of publications. The central idea is that either disorder[5–8] or electron-electron interaction[9–12] may affect the value of the minimal conductivity. Moreover, the value of minimal conductivity at low temperatures depends on the order of various limits (e.g., frequency $\omega \to 0$ and temperature $T \to 0$) and is related to the scaling property $\sigma_{\min}(\omega,T) = \sigma_{\min}(\omega/T)$.[13] Below we employ the zero-temperature formalism which suggests $T \to 0$ and $\omega \to 0$. This yields for the dc limit of the ac conductivity the value $\pi/2$.[7,9,13]

An additional problem in terms of disorder is that it is not clear what role is played by different types of disorder. Since disorder, depending on its type, may break different internal symmetries of the Dirac Hamiltonian, a classification according of the different types is crucial. On the other hand, the origin of disorder in graphene can be different. In addition to impurities inside the graphene sheet and in the substrate, the deformation of the lattice (e.g., ripples) might be the main source of disorder.[14–16] In general, it is believed that surface corrugations[11,17,18] may influence the electronic transport properties of graphene. It is crucial to notice that lattice deformations do not break the chiral symmetry at the Dirac point, in contrast to potential disorder or a random gap caused by a random deposition of hydrogen.[19] Therefore, it is expected that this type of disorder has a rather weak effect on

transport properties.[20] This is supported by calculations where the lattice deformations are approximated by an uncorrelated random vector potential in the Dirac Hamiltonian.[21] This type of disorder has no effect on the minimal conductivity.[5] More recently, however, a more general theory of lattice deformations with long-range correlations revealed a dramatic increase of the minimal conductivity for weak disorder.[17] In this paper, we study a similar model by an alternative approach to check whether or not this dramatic increase of the minimal conductivity can be reproduced.

First we consider the deformation of the graphene sheet in three dimensions and show that in the continuum limit the dynamics of the electrons on the two-dimensional surface is defined by the so-called induced Dirac action presented in Ref. 22. In our approach the internal deformations of the graphene sheet and the deformations perpendicular to the sheet direction are unified into one schema, while in the approach developed in Refs. 17, 21, and 23–25 there are separate internal (2D) gravity and additional non-Abelian gauge fields. The deformations of the sheet in three dimensions by local SO(3) rotations of the basic vectors in our approach carry the degrees of freedom of the additional gauge field.

Then we develop a replica-trick-based field theory to take the random character of surfaces into account and to calculate the average optical conductivity by a perturbative expansion. Our main result is that the random lattice deformations do not affect the robust character of minimal conductivity, contrary to the result presented in Ref. 17.

II. THE MODEL

We depart from a model of hopping fermions on the regular 2D honeycomb lattice. A honeycomb lattice has a natural partition into two triangular sublattices and we mark electronic fields associated with sites of the sublattices as $(\bar{\psi}_{\vec{n},\alpha}, \psi_{\vec{n},\alpha})$, $\alpha = 1,2$. The action of electrons hopping on a line with the lattice spacing $|\vec{e}|$ reads

$$\mathcal{S}[\bar{\psi},\psi] = i \sum_{t,\vec{n}} (\bar{\psi}_{t,\vec{n}} \gamma_0 \partial_t \psi_{t,\vec{n}} + \bar{\psi}_{t,\vec{n}} \gamma_2 \psi_{t,\vec{n}+\vec{e}}),$$

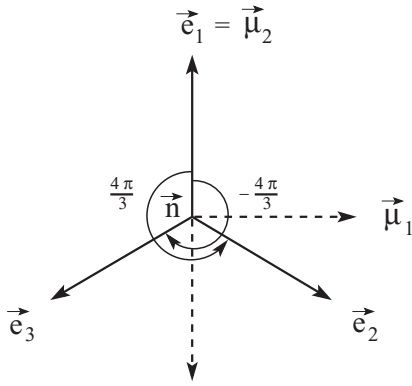but when fermions change hopping direction in two-dimensional space, the fields should also be rotated by a

FIG. 1. Hopping vectors on a regular honeycomb lattice.

corresponding angle (Fig. 1). On the honeycomb lattice (Fig. 2), we have

$$
\mathcal{S}[\bar{\Psi}, \Psi] = i \sum_{t,\vec{n},i} \left(\bar{\Psi}_{t,\vec{n}} \gamma_0 \partial_t \Psi_{t,\vec{n}} + \bar{\Psi}_{t,\vec{n}} \gamma_2 \Psi'_{t,\vec{n}+\vec{e}_i} \right),
$$

$$
\Psi_{t,\vec{n}} = \begin{pmatrix} \psi_{t,\vec{n},1} \\ \psi_{t,\vec{n},2} \end{pmatrix}, \qquad i = 1,2,3, \tag{1}
$$

where γ_0, γ_j ($j = 1,2$) are Dirac matrices which are related to usual Pauli matrices via $\gamma_1 = \sigma_2$, $\gamma_2 = -\sigma_1$, and $\gamma_0 = \sigma_3$ and fields

$$
\Psi'_{\vec{n}+\vec{e}_1} = \Psi_{\vec{n}+\vec{e}_1} = e^{\vec{e}_1 \cdot \vec{\partial}} \Psi_{\vec{n}}, \tag{2a}
$$

$$
\Psi'_{\vec{n}+\vec{e}_2} = e^{i \frac{2\pi}{3} \gamma_0} \Psi_{\vec{n}+\vec{e}_2} = e^{i \frac{2\pi}{3} \gamma_0} e^{\vec{e}_2 \cdot \vec{\partial}} \Psi_{\vec{n}}, \tag{2b}
$$

$$
\Psi'_{\vec{n}+\vec{e}_3} = e^{-i \frac{2\pi}{3} \gamma_0} \Psi_{\vec{n}+\vec{e}_3} = e^{-i \frac{2\pi}{3} \gamma_0} e^{\vec{e}_3 \cdot \vec{\partial}} \Psi_{\vec{n}}, \tag{2c}
$$

are rotated by $\pm 4\pi/3$ and translated by $\vec{e}_{2,3}$ spinor representations of the rotation group SO(3). In the paper by Semenoff,[26] it was shown that the spectrum of low-energy excitations of the hopping fermions on a honeycomb lattice (corresponding to the continuum limit of the model) coincides with the spectrum of Dirac fermions in three-dimensional (3D) space. Below we show that the continuum limit of the action of fermions hopping on a honeycomb lattice, Eq. (1), is defined by the Dirac action in three-dimensional coordinate space. This allows us
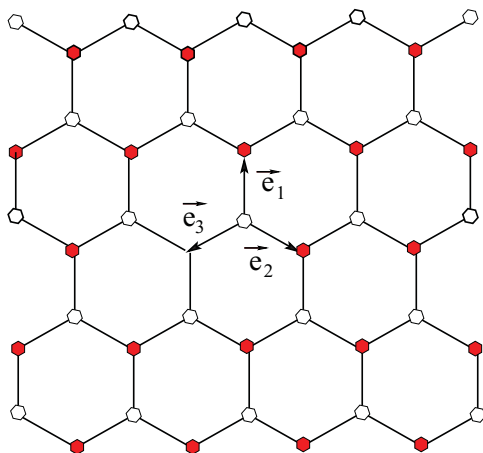
to construct the continuum limit of the generalized hopping model on the randomly deformed lattice.

In order to find a continuum limit of the action Eq. (1), one expands the translational operators $e^{\vec{e}_i \cdot \vec{\partial}} \simeq 1 + \vec{e}_i \cdot \vec{\partial}$ and substitutes Eq. (2a) for Ψ's into the action Eq. (1). Then after some simple algebra one obtains

$$
\mathcal{S} = i \sum_{t,\vec{n}} \bar{\Psi}_{t,\vec{n}} \left(\gamma_0 \partial_t + \frac{3}{4} \gamma^i \vec{\mu}_i \cdot [\overleftarrow{\partial} - \overrightarrow{\partial}] \right) \Psi_{t,\vec{n}} \tag{3}
$$

$$
\rightarrow i \int d^2\xi \, dt \, \bar{\Psi} \left(\gamma_0 \partial_t + \frac{1}{2} \gamma^i \vec{\mu}_i \cdot [\overleftarrow{\partial} - \overrightarrow{\partial}] \right) \Psi, \tag{4}
$$

where we introduced orthonormalized vectors $\vec{\mu}_1 = (\vec{e}_2 - \vec{e}_3)/\sqrt{3}$ and $\vec{\mu}_2 = \vec{e}_1$. In line (4), we have rescaled the fields and coordinates as $\Psi \rightarrow 2/3\Psi, \xi \rightarrow 3\xi/2, t \rightarrow t$, and $\mu_i \rightarrow \mu_i$. It is clear from Eq. (4) that vectors $\vec{\mu}_a = \mu_a^i(\vec{\xi})\hat{e}_i$ ($a = 1,2$), with $\hat{e}_i$ ($i = 1,2$), representing an orthonormal basis in the flat space play the role of tetrads (vielbein) in a 2D plane with arbitrary coordinates ξ_i ($i = 1,2$). Indeed, consider deformation of the honeycomb lattice (cf. Fig. 3) and attach to the sites new coordinates ξ_i'. Then the vectors μ_a^i ($a = 1,2, i = 1,2$) are connected with the same vectors in the old coordinate ξ_i ($i = 1,2$) via

$$
\mu_a^i(\vec{\xi}) = \frac{\partial \xi_j'}{\partial \xi_i} \mu_a^j(\vec{\xi}'). \tag{5}
$$

We now regard the vectors μ_i^a as vielbeins in a 2D plane which obey the orthogonality relation $\mu_i^a \mu_{a,j} = \delta_{ij}$ and we define the metric $\mu_i^a \mu_j^a = g_{ij}$. After integration by parts in Eq. (3) and using the relation $\hat{\mu}_i \hat{\mu}_j = g_{ij} + \frac{i}{\sqrt{g}} \epsilon_{ij} \gamma_0$ with $\hat{\mu}_i = \gamma^a \mu_i^a$ and $g = \det[g_{ij}]$, one obtains

$$
\mathcal{S}[\bar{\Psi}, \Psi]
$$

$$
= i \int d^2\xi \, dt \, \bar{\Psi} \left(\gamma_0 \partial_t + \gamma^a \mu_a^j \left[\partial_j - \frac{i}{2} \gamma_0 \Gamma_j \right] \right) \Psi, \tag{6}
$$

where $\Gamma_j = \frac{i}{2\sqrt{g}} \epsilon_{ab} \mu_a^k \nabla_j \mu_{k,b}$ is a standard spinor connection corresponding to the vielbein μ_a^j and ∇_j denotes a covariant derivative. For a scalar function f it reduces to a usual partial derivative, $\nabla_i f = \partial_i f$, while for a vector-valued function f_j
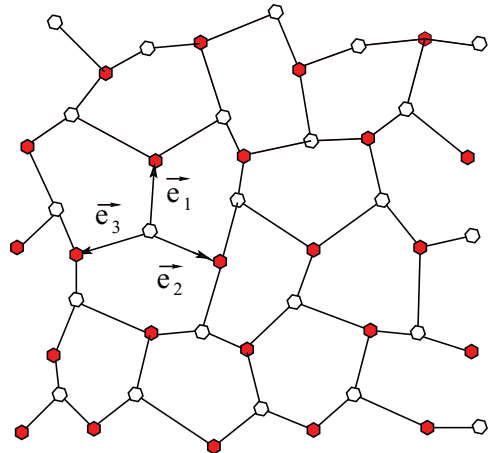

FIG. 2. (Color online) Regular honeycomb lattice.

FIG. 3. (Color online) Random honeycomb lattice.

it is $\nabla_i f_j = \partial_i f_j + \Gamma^k_{ij} f_k$, where Γ^k_{ij} represent Christoffel symbols.

An important remark is necessary here. The spinor connection Γ_j, given following Eq. (6), is defined up to a local U(1)-gauge transformation related to the rotation of the vielbeins μ^k_a in the tangential plane. On compact surfaces (e.g., a torus), such gauge transformations may have a nontrivial boundary contribution which can create field configurations with a nontrivial topology. This situation is typical for the topological insulators. However, here we do not consider compact spaces, and such types of topological boundary effects are not relevant for our analysis.

Let us now consider deformations of the honeycomb lattice in a three-dimensional space.[22,27] This means that two γ_a ($a = 1,2$) matrices in a tangent plane become γ matrices in a SO(3) rotated plane which is tangent to a curved surface at the point ξ_i:

$$\hat{x}_a(\xi_i) = U(\xi_i)^{-1} \gamma_a U(\xi_i). \qquad (7)$$

As shown in Ref. 22, local rotations by $U(\vec{\xi})$ produce a 2D surface embedded in 3D Euclidean space if

$$U^{-1} \partial_\mu U = \tfrac{1}{4}(\hat{x}_a \partial_\mu \hat{x}_a + \hat{n} \partial_\mu \hat{n}), \qquad (8)$$

where $\hat{x}_a = \mu^\mu_a \partial_\mu x^\alpha \gamma_\alpha$ and $\hat{n} = n^\alpha \gamma_\alpha$ ($\alpha = 0,1,2$) being the tangent and normal to the surface 3D vectors at the point ξ, respectively. This occurs because Eq. (8) fulfills the Gauss-Codazzi equations,[27,28] which represent the necessary conditions for the surface x^α to be embedded in 3D Euclidean space.

Then we should also rotate fermionic fields by the same matrices $\Psi \to U\Psi$, after which the action becomes

$$S = i \int d^2\xi \, dt \, \bar{\Psi} U^{-1} \left(\gamma_0 \partial_t + \gamma^a \mu^\mu_a \left[\partial_\mu - \tfrac{i}{2} \gamma_0 \Gamma_\mu \right] \right) U\Psi, \qquad (9)$$

where $\Gamma_\mu = i \mathrm{Tr}(\hat{n} U^{-1} \partial_\mu U)$ is the spinor connection on the surface x^α. By use of Eq. (7), this expression can be simplified essentially (see details in Refs. 22 and 27), acquiring the form

$$S[\bar{\Psi}, \Psi] = i \int d^2\xi \, dt \, \bar{\Psi} \left(\gamma_0 \partial_t + \tfrac{1}{2} \sqrt{g} \hat{\gamma}^\mu [\overleftarrow{\partial_\mu} - \overrightarrow{\partial_\mu}] \right) \Psi, \qquad (10)$$

where

$$g_{\nu\mu} = \partial_\nu \mathbf{x} \cdot \partial_\mu \mathbf{x} = \partial_\nu x^\alpha \partial_\mu x_\alpha \qquad (11)$$

is the metric on the surface $x^\alpha(\vec{\xi})$ induced by its embedding in 3D Euclidean space, g denotes its determinant, and

$$\hat{\gamma}^\mu = \partial^\mu \mathbf{x} \cdot \gamma = \partial^\mu x^a \gamma_a \qquad (12)$$

represents the induced Dirac matrices.[22] In a flat space, i.e., for $\mathbf{x}(\vec{\xi}) = \mathbf{x}_0 + \hat{\mathbf{e}}^\mu \xi_\mu$, the induced metric reduces to a usual diagonal matrix. One can call action Eq. (10) the induced Dirac action since the matrices $\hat{\gamma}^\mu$ are induced by embedding. The expression in Eq. (10) is a generalization of 2D action Eq. (4) to 3D space.

III. EFFECTIVE ACTION FOR SMALL CORRUGATIONS

Performing integration by parts in Eq. (10), we arrive at

$$S = i \int d^2\xi \, dt \, \bar{\Psi}(\gamma_0 \partial_t + \sqrt{g} \hat{\gamma}^\mu [\partial_\mu + \Gamma_\mu])\Psi. \qquad (13)$$

Here, the quantity

$$\Gamma_\mu = \tfrac{1}{2} \hat{\gamma}^\nu \nabla_\mu \hat{\gamma}_\nu \qquad (14)$$

plays the role of an induced spinor connection, where ∇_μ denotes the operator of covariant differentiation and is defined as[22,27]

$$\nabla_\mu(\cdots) = \frac{1}{\sqrt{g}} \partial_\mu(\sqrt{g} \cdots).$$

Let us derive the asymptotic action for small corrugations of the graphene sheet. In this case the surface $\mathbf{x}$ can be asymptotically represented as

$$\mathbf{x}(\xi_1, \xi_2) \approx \mathbf{x}_0 + \hat{\mathbf{e}}^\mu \xi_\mu + \mathbf{x}'(\xi_1, \xi_2). \qquad (15)$$

Plugging Eq. (15) into Eq. (11), we obtain the asymptotics of the metric tensor:

$$g_{\nu\mu} \approx \delta_{\nu\mu} + \epsilon_{\nu\mu} + \epsilon_{\mu\nu}, \qquad (16)$$

where

$$\epsilon_{\nu\mu} = \hat{\mathbf{e}}_\nu \cdot \partial_\mu \mathbf{x}'. \qquad (17)$$

Thus the metric tensor is in general neither diagonal nor symmetric. Its determinant is found using the common relations

$$g \approx 1 + 2\epsilon_{11} + 2\epsilon_{22} = 1 + 2\epsilon_{\nu\nu}, \qquad (18)$$

and correspondingly its square root is

$$\sqrt{g} \approx 1 + \epsilon_{\nu\nu}. \qquad (19)$$

Using Eqs. (12), (15), and (19), we arrive at the effective action for small fluctuations ϵ:

$$S_0[\bar{\Psi}, \Psi; \epsilon] \approx i \int d^2\xi \, dt \, \bar{\Psi}(\gamma_0 \partial_t + [1 + \epsilon_{\nu\nu}]\tilde{\gamma}^\mu \partial_\mu)\Psi$$
$$+ \frac{i}{2} \int d^2\xi \, dt \, \bar{\Psi} \tilde{\gamma}^\mu \partial_\mu \epsilon_{\nu\nu} \Psi, \qquad (20)$$

with induced γ matrices $\tilde{\gamma}^\mu = e^\mu_a \gamma^a$. For further purposes, we associate the spatial fluctuations with a bosonic field,

$$\epsilon_{\nu\nu} = \Lambda(\vec{\xi}, t),$$

and its gradient with a static vector-disorder-like term:

$$\partial_\mu \epsilon_{\nu\nu} = \partial_\mu \Lambda(\vec{\xi}, t) = B_\mu(\vec{\xi}, t).$$

Hence the action formally becomes

$$S_0[\bar{\Psi}, \Psi; \Lambda, \mathbf{B}] \approx i \int d^2\xi \, dt \, \bar{\Psi}(\gamma_0 \partial_t + \tilde{\gamma}^\mu \partial_\mu)\Psi$$
$$+ i \int d^2\xi \, dt \, \Lambda \bar{\Psi} \tilde{\gamma}^\mu \partial_\mu \Psi$$
$$+ \frac{i}{2} \int d^2\xi \, dt \, \bar{\Psi} \tilde{\gamma}^\mu B_\mu \Psi. \qquad (21)$$

The action derived this way reproduces the ansatz action considered in Ref. 17.

Below we consider topologic defects in the flat space. Technically that means that we replace zweibeins e_a^μ by a unity matrix. We are ultimately interested in the effect of this sort of the disorder on the optical conductivity. In order to perform such calculations we have to make some suggestions regarding the correlators of the introduced quantities. One usually requires the vector disorder fields B_μ to be Gaussian correlated, i.e.,

$$\langle B_\mu(\vec{\xi},t)\rangle = 0, \tag{22}$$

$$\langle B_\mu(\vec{\xi},t)B_\nu(\vec{\xi}',t')\rangle = g_0^2 \delta_{\mu\nu}\delta(t)\delta(t')\delta(\vec{\xi}-\vec{\xi}'), \tag{23}$$

which guarantees that the vector associated with the random disorder is static. In Fourier space these expressions read with the shorthand $Q = (q_0, \boldsymbol{q})$:

$$\langle B_\mu(Q)\rangle = 0, \tag{24}$$

$$\langle B_\mu(Q)B_\nu(Q')\rangle = g_0^2(2\pi)^2 \delta_{\mu\nu}\delta(\boldsymbol{q}+\boldsymbol{q}'). \tag{25}$$

From Eqs. (23) and (25), we are led to the correlators of the scalars Λ, since we have an exact relationship

$$\langle B_\mu(Q)B_\nu(Q')\rangle = i^2 q_\mu q'_\nu \langle \Lambda(Q)\Lambda(Q')\rangle, \tag{26}$$

which leads to

$$\langle \Lambda(Q)\Lambda(Q')\rangle = \frac{g_0^2}{q^2+\mu^2}(2\pi)^2\delta(\boldsymbol{q}+\boldsymbol{q}'), \tag{27}$$

where we have introduced an infrared cutoff μ of the order of the inverse lattice spacing in order to avoid long-wavelength divergences. The inverse Fourier transform yields, for the $\langle \Lambda\Lambda \rangle$ correlator,

$$\langle \Lambda(\vec{\xi},t)\Lambda(\vec{\xi}',t')\rangle = g_0^2\delta(t)\delta(t')\log|\mu(\vec{\xi}-\vec{\xi}')|. \tag{28}$$

The disorder propagator in Eq. (27) depends only on the spatial momenta $\boldsymbol{q}$ and $\boldsymbol{q}'$ and a 2D integration should be performed when averaging over them. In order to keep our 3D notation uniform, we augment Eq. (27) by a δ function of both frequencies q_0 and q_0':

$$\langle \Lambda(Q)\Lambda(Q')\rangle = \frac{g_0^2}{q^2+\mu^2}(2\pi)^4\delta(q_0)\delta(Q+Q'). \tag{29}$$

Furthermore, we always assume

$$\langle \Lambda(\vec{\xi},t)\rangle = \langle \Lambda(Q)\rangle = 0. \tag{30}$$

The Fourier transform of Eq. (20) expressed in terms of the scalar fields Λ only reads

$$\mathcal{S}[\bar{\Psi},\Psi,\Lambda] = -\int_Q \bar{\Psi}_Q(q_0\gamma_0+\gamma\cdot\boldsymbol{q})\Psi_Q$$
$$- \int_Q\int_P \Lambda_P\bar{\Psi}_{P+Q}\Gamma(P+Q,P,Q)\Psi_Q, \tag{31}$$

where $\gamma\cdot\boldsymbol{q} = \gamma^\mu q_\mu$. The two-particle vertex is obtained from Eq. (31) in the limit $\Lambda\to 0$ by performing a second-order functional derivative with respect to the Grassmann fields:

$$\Gamma(P,Q) = (2\pi)^3\delta(P-Q)G_0^{-1}(Q), \tag{32}$$

where

$$G_0^{-1}(Q) = q_0\gamma_0+\gamma\cdot\boldsymbol{q} \tag{33}$$

represents the inverse free propagator and correspondingly

$$G_0(Q) = \frac{q_0\gamma_0+\gamma\cdot\boldsymbol{q}}{q_0^2+q^2} \tag{34}$$

the free Dirac propagator. The three-particle vertex function $\Gamma(K_{\bar\Psi},K_\Lambda,K_\Psi)$ follows from Eq. (31):

$$\Gamma(K_{\bar\Psi};K_\Lambda,K_\Psi) = (2\pi)^3\delta(K_{\bar\Psi}-K_\Lambda-K_\Psi)$$
$$\times \tfrac{1}{2}\gamma\cdot(\boldsymbol{k}_\Lambda+2\boldsymbol{k}_\Psi). \tag{35}$$

Furthermore, we have to augment Eq. (31) by the interaction between fermions and the radiation field,

$$\mathcal{S}_{\rm opt}[\bar{\Psi},\Psi,A] = -\int_P\int_Q A_P\bar{\Psi}_{P+Q}\gamma_0\Psi_Q, \tag{36}$$

which suggests the presence of an electric field applied to the graphene sheet. Interaction Eq. (36) gives rise to the optical conductivity due to polarization of the charge carriers. The corresponding bare vertex is defined as

$$\Gamma_0(K_{\bar\Psi},K_A,K_\Psi) = (2\pi)^3\delta(K_{\bar\Psi}-K_A-K_\Psi)\gamma_0. \tag{37}$$

The full action acquires the form

$$\bar{\mathcal{S}}[\bar{\Psi},\Psi,\Lambda,A] = \mathcal{S}[\bar{\Psi},\Psi,\Lambda] + \mathcal{S}_{\rm opt}[\bar{\Psi},\Psi,A]. \tag{38}$$

The electron-gauge boson interaction renormalizes the electronic spectrum and therefore should have an effect on the response to the radiation field.

IV. OPTICAL CONDUCTIVITY OF GRAPHENE

We consider first clean graphene. The corresponding Euclidean action is obtained from Eq. (38) if we assume $\Lambda = 0$:

$$\mathcal{S}_0[\bar{\Psi},\Psi;A] = -\int_Q \bar{\Psi}_Q(q_0\gamma_0+\gamma\cdot\boldsymbol{q})\Psi_Q$$
$$- \int_P\int_Q A(P-Q)\bar{\Psi}_P\gamma_0\Psi_Q. \tag{39}$$

The optical conductivity of a 2D Dirac electron gas can be calculated from the electronic polarization [9,12]

$$\sigma_0 = 4k_0\lim_{k\to 0}\frac{1}{2}\frac{\partial^2}{\partial k^2}\Pi(K), \tag{40}$$

where $\Pi(K)$ denotes the irreducible polarization. The factor 4 in front of this expression arises from taking both spin and valley degeneracy into account. To leading order it is given by the diagram shown in Fig. 4. Algebraically we have for the polarization bubble

$$\Pi(K) = \int_P \mathrm{Tr}\{\gamma_0 G_0(P)\gamma_0 G_0(K+P)\}, \tag{41}$$
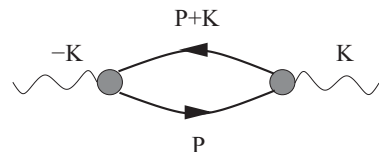

FIG. 4. Bare polarization bubble.

with the bare Dirac propagators $G_0(Q)$ defined in Eq. (34). We give some details of the calculation in the Appendix. The irreducible polarization is obtained as

$$\Pi(K) = \frac{1}{16} \frac{k^2}{\sqrt{k^2 + k_0^2}}, \tag{42}$$

and the optical conductivity in SI units is

$$\sigma_0 = \frac{1}{4} \frac{e^2}{\hbar} = \frac{\pi}{2} \frac{e^2}{h}. \tag{43}$$

In what follows we calculate corrections of the conductivity in Eq. (43) due to lattice deformations described in Sec. III. To leading order in momenta the renormalized inverse fermionic propagator can be written as

$$G^{-1}(Q) = G_0^{-1}(Q) - \Sigma(Q) \approx Z_0^{-1} q_0 \gamma_0 + Z_1^{-1} \gamma \cdot \boldsymbol{q} \tag{44}$$

with renormalization factors

$$Z_{0,1}^{-1} = 1 - \gamma_{0,\mu} \frac{\partial}{\partial q_{0,\mu}} \Sigma(Q)|_{Q=0}$$

$$= \gamma_{0,\mu} \frac{\partial}{\partial q_{0,\mu}} G^{-1}(Q)|_{Q=0}, \tag{45}$$

where $\Sigma(Q)$ denotes the fermionic self-energy. However, the dressed electron-photon vertex can be written in the following form:

$$\tilde{\Gamma}_0(Q) \approx \tilde{e} \gamma_0 + O(Q), \tag{46}$$

where $\tilde{e}$ denotes the renormalization of the elementary charge due to lattice deformations, such that the effective renormalized action reads

$$\tilde{\mathcal{S}}_0[\bar{\Psi}, \Psi; A] \approx - \int_Q \bar{\Psi}_Q \left(Z_0^{-1} q_0 \gamma_0 + Z_1^{-1} \gamma \cdot \boldsymbol{q} \right) \Psi_Q$$

$$- \tilde{e} \int_P \int_Q A(P - Q) \bar{\Psi}_P \gamma_0 \Psi_Q. \tag{47}$$

The effect of the lattice defects on the optical conductivity can be calculated from the dressed polarization shown in Fig. 5. The dressing effect of the lattice defects is taken into account by replacing the bare Green's functions G_0 in Fig. 4 by the full propagators G defined in Eq. (44) and bare vertices γ_0 by the dressed ones $\tilde{\Gamma}_0$ from Eq. (46). Algebraically we obtain

$$\tilde{\Pi}(K) = \int_P \text{Tr}\{\tilde{\Gamma}_0 G(P) \tilde{\Gamma}_0 G(K + P)\}$$

$$= \frac{2\tilde{e}^2}{Z_0^{-2}} \int_P \frac{p_0(p_0 + k_0) - \alpha^2 \boldsymbol{p} \cdot (\boldsymbol{p} + \boldsymbol{k})}{[p_0^2 + \alpha^2 p^2][(p_0 + k_0)^2 + \alpha^2 (\boldsymbol{k} + \boldsymbol{p})^2]}, \tag{48}$$
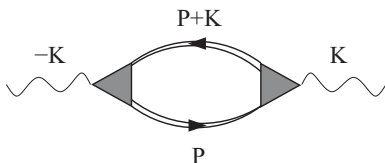
where $\alpha = Z_1^{-1}/Z_0^{-1}$. The integration can be performed with some effort, but we restrict our attempts to a more direct task; i.e., we calculate only the modified optical conductivity $\tilde{\sigma}$ analogously to the optical conductivity of clean graphene as we did before. We take the derivative with respect to k under the integral and employ the residue theorem in order to integrate out loop frequency p_0. At the end of the calculation we arrive at

$$\tilde{\sigma} = \tilde{e}^2 Z_0^2 \sigma_0. \tag{49}$$

Surprisingly, apart from the vertex renormalization, only renormalization of the frequency contributes to the modified conductivity. Therefore, our task reduces to the calculation of the renormalization factors Z_0 and $\tilde{e}$, which is performed perturbatively below.

V. CALCULATION OF RENORMALIZATION FACTORS

In order to set up perturbative calculations, we have to average over the lattice deformations. There are two possible ways to implement such averaging: the replica-trick and the supersymmetry approach. The calculation below is based on the replica-trick approach.

According to the replica trick, we introduce N copies of fermions Ψ^α ($\alpha = 1, 2, \ldots, N$) with the same action:

$$\bar{\mathcal{S}} = - \int_Q \bar{\Psi}_Q^\alpha (q_0 \gamma_0 + \gamma \cdot \boldsymbol{q}) \Psi_Q^\alpha$$

$$- \int_Q \int_P \Lambda_P \bar{\Psi}_{P+Q}^\alpha \Gamma(P + Q, P, Q) \Psi_Q^\alpha$$

$$- \int_Q \int_P A_P \bar{\Psi}_{P+Q}^\alpha \gamma_0 \Psi_Q^\alpha. \tag{50}$$

Then we calculate the diagrams describing renormalization of the fermionic propagator and electron-photon vertex function and perform the limit $N \to 0$ at the end of the calculation. As the result of this procedure, all contributions containing factors proportional to any positive power of N vanish. These include, for instance, contributions arising from diagrams containing closed fermionic loops.

The diagrams of the fermionic self-energy to the order 1 in replicas indices and to order g_0^4 in lattice deformation strengths are shown in Figs. 6 and 7. Correspondingly, the same order diagrams of vertex corrections are depicted in Figs. 8 and 9. Retaining only frequency dependence ($\boldsymbol{p} = 0$) in the analytical expressions for these contributions, we obtain for the leading self-energy contribution (Fig. 6)

$$\Sigma^{(2)}(p_0) = \frac{g_0^2}{4} \int_q \Gamma_1 G_0(p_0, \boldsymbol{q}) \Gamma_2 F(\boldsymbol{q}), \tag{51}$$
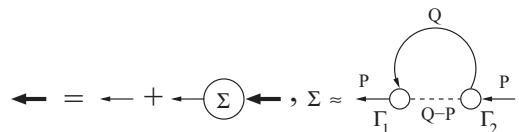

FIG. 5. Dressed polarization bubble.

FIG. 6. Dressed fermionic Green's function and leading-order diagram of the fermionic self-energy. Dashed lines denote the $\langle \Lambda \Lambda \rangle$ correlator and open circles the $\bar{\Psi} \Lambda \Psi$ vertices.
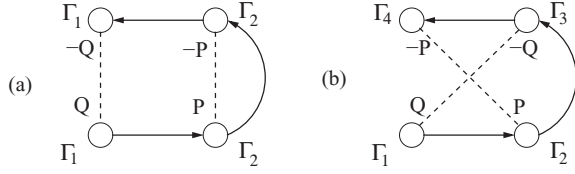
FIG. 7. Second-order self-energy corrections at zero external momenta.

where $\Gamma_1 = \Gamma_2 = \gamma \cdot \boldsymbol{q}$, and

$$F(\boldsymbol{q}) = \frac{1}{q^2 + \mu^2} \tag{52}$$

denotes the momentum-dependent part of the $\langle \Lambda \Lambda \rangle$ correlator defined in Eq. (28). The diagram of the next order in g_0 depicted in Fig. 7(a) reads

$$\Sigma_1^{(2)}(p_0) = \frac{g_0^4}{16} \int_q F(\boldsymbol{q}) \int_p F(\boldsymbol{p}) \Gamma_1 G_0(p_0, q) \Gamma_2$$
$$\times G_0(p_0, \boldsymbol{q} + \boldsymbol{p}) \Gamma_2 G_0(p_0, \boldsymbol{q}) \Gamma_1,$$

where $\Gamma_1 = \gamma \cdot \boldsymbol{q}$ and $\Gamma_2 = \gamma \cdot (2\boldsymbol{q} + \boldsymbol{p})$, while the diagram shown in Fig. 7(b) gives

$$\Sigma_2^{(2)}(p_0) = \frac{g_0^4}{16} \int_q F(\boldsymbol{q}) \int_p F(\boldsymbol{p}) \Gamma_1 G_0(p_0, q) \Gamma_2$$
$$\times G_0(p_0, \boldsymbol{q} + \boldsymbol{p}) \Gamma_3 G_0(p_0, \boldsymbol{p}) \Gamma_4,$$

with the vertices $\Gamma_1 = \gamma \cdot \boldsymbol{q}$, $\Gamma_2 = \gamma \cdot (2\boldsymbol{q} + \boldsymbol{p})$, $\Gamma_3 = \gamma \cdot (2\boldsymbol{p} + \boldsymbol{q})$, and $\Gamma_4 = \gamma \cdot \boldsymbol{p}$. Eventually, for the contributions to the wave-function renormalization factor, we obtain

$$\frac{\partial}{\partial p_0} \Sigma^{(2)}(p_0)|_{p_0=0} = -\hat{e}, \tag{53}$$

$$\frac{\partial}{\partial p_0} \Sigma_1^{(4)}(p_0)|_{p_0=0} = -9\hat{e}^2, \tag{54}$$

$$\frac{\partial}{\partial p_0} \Sigma_2^{(4)}(p_0)|_{p_0=0} = -\frac{15}{2}\hat{e}^2, \tag{55}$$

where we define

$$\hat{e} = \frac{g_0^2}{8\pi} \log \frac{\lambda}{\mu}, \tag{56}$$

with λ denoting some upper momentum cutoff. Therefore, for the wave-function renormalization to the second order in g_0^2, we obtain

$$Z_0^{-1} \approx 1 + \hat{e} + \frac{33}{2}\hat{e}^2 + O(\hat{e}^3). \tag{57}$$

Now we look at the renormalization of the electron-photon vertex function. Diagrammatically the leading-order
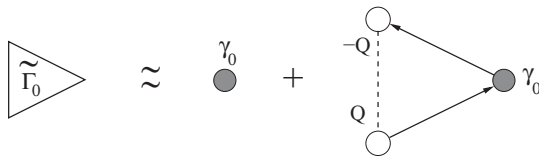

FIG. 8. Leading-order perturbative contribution to the amputated electron-phonon coupling vertex. Dashed lines denote the $\langle \Lambda \Lambda \rangle$ correlator and open circles the $\bar{\Psi} \Lambda \Psi$ vertices.

correction is given by the second term on the right-hand side of the diagram shown in Fig. 8. According to Eq. (49), the main corrections to the conductivity arise from the momentum-independent part of the vertex function. We obtain for the vertices $\Gamma_1 = \Gamma_2 = \gamma \cdot \boldsymbol{q}$. The algebraic expression for the diagram depicted in Fig. 8 is given by

$$\tilde{\Gamma}^{(1)}(0) = \frac{g_0^2}{4} \int_q \Gamma_1 G_0(\boldsymbol{q}) \Gamma_0 G_0(\boldsymbol{q}) \Gamma_2 F(\boldsymbol{q}), \tag{58}$$

which yields, after the evaluation,

$$\tilde{\Gamma}^{(1)}(0) = \hat{e} \gamma_0, \tag{59}$$

where $\hat{e}$ from Eq. (56) is introduced and acquires the meaning of the leading-order elementary charge renormalization.

Second-order vertex corrections can be calculated from the diagrams shown in Fig. 9. Due to the mirror symmetry, Figs. 9(c) and 9(d) depicted in the second row should be counted twice. Let us first consider the contribution that arises from the diagram depicted in Fig. 9(a) with two parallel ladder rungs. At zero external momenta, we obtain for the vertices $\Gamma_1 = \Gamma_4 = \gamma \cdot \boldsymbol{q}$ and $\Gamma_2 = \Gamma_3 = \gamma \cdot (2\boldsymbol{q} + \boldsymbol{p})$. We obtain for the correction

$$\tilde{\Gamma}_1^{(2)}(0) = \frac{g_0^4}{16} \int_q F(\boldsymbol{q}) \int_p F(\boldsymbol{p}) \Gamma_1 G_0(\boldsymbol{q}) \Gamma_2 G_0(\boldsymbol{p} + \boldsymbol{q})$$
$$\times \Gamma_0 G_0(\boldsymbol{p} + \boldsymbol{q}) \Gamma_2 G_0(\boldsymbol{q}) \Gamma_1, \tag{60}$$

which, after performing integrations, yields

$$\tilde{\Gamma}_1^{(2)}(0) = 2\hat{e}^2 \gamma_0. \tag{61}$$

For Figs. 9(b), 9(c), and 9(d), we proceed similarly. In the case of Fig. 9(b), we have the following expressions for the vertices: $\Gamma_1 = \gamma \cdot \boldsymbol{q}$, $\Gamma_2 = \gamma \cdot (2\boldsymbol{q} + \boldsymbol{p})$, $\Gamma_3 = \gamma \cdot (2\boldsymbol{p} + \boldsymbol{q})$, and $\Gamma_4 = \gamma \cdot \boldsymbol{p}$. Therefore, the expression for this correction reads

$$\tilde{\Gamma}_2^{(2)}(0) = \frac{g_0^4}{16} \int_q F(\boldsymbol{q}) \int_p F(\boldsymbol{p}) \Gamma_1 G_0(\boldsymbol{q}) \Gamma_2 G_0(\boldsymbol{p} + \boldsymbol{q})$$
$$\times \Gamma_0 G_0(\boldsymbol{p} + \boldsymbol{q}) \Gamma_3 G_0(\boldsymbol{p}) \Gamma_4, \tag{62}$$

with the result

$$\tilde{\Gamma}_2^{(2)}(0) = \frac{5}{2}\hat{e}^2 \gamma_0. \tag{63}$$

For Fig. 9(c), we have the following vertices: $\Gamma_1 = \gamma \cdot \boldsymbol{q}$, $\Gamma_2 = \gamma \cdot (2\boldsymbol{q} + \boldsymbol{p})$, $\Gamma_3 = \gamma \cdot (2\boldsymbol{p} + \boldsymbol{q})$, and $\Gamma_4 = \gamma \cdot \boldsymbol{p}$, whereas the expression for the correction reads

$$\tilde{\Gamma}_3^{(2)}(0) = \frac{g_0^4}{16} \int_q F(\boldsymbol{q}) \int_p F(\boldsymbol{p}) \Gamma_1 G_0(\boldsymbol{q}) \Gamma_0 G_0(\boldsymbol{q}) \Gamma_2$$
$$\times G_0(\boldsymbol{p} + \boldsymbol{q}) \Gamma_3 G_0(\boldsymbol{p}) \Gamma_4, \tag{64}$$

which yields the result

$$\tilde{\Gamma}_3^{(2)}(0) = \frac{5}{2}\hat{e}^2 \gamma_0. \tag{65}$$

Finally, Fig. 9(d) an be written algebraically as follows:

$$\tilde{\Gamma}_4^{(2)}(0) = \frac{g_0^4}{16} \int_q F(\boldsymbol{q}) \int_p F(\boldsymbol{p}) \Gamma_1 G_0(\boldsymbol{q}) \Gamma_0 G_0(\boldsymbol{q}) \Gamma_2$$
$$\times G_0(\boldsymbol{p} + \boldsymbol{q}) \Gamma_3 G_0(\boldsymbol{q}) \Gamma_4, \tag{66}$$
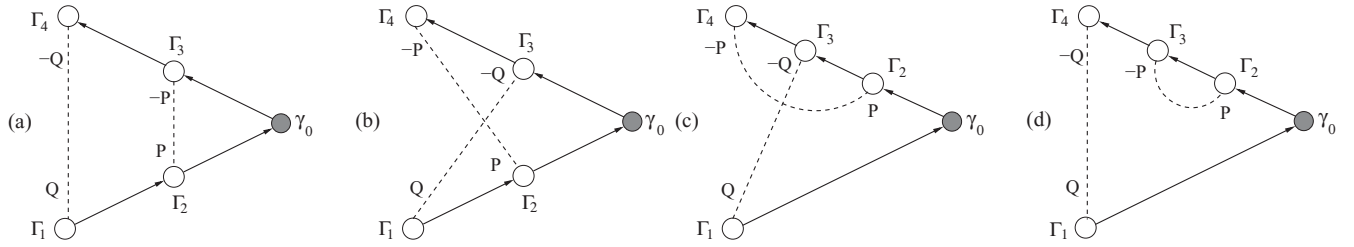
FIG. 9. Second-order vertex correction diagrams at zero external momenta. The diagrams in the second row should be counted twice due to the mirror symmetry.

where the vertices $\Gamma_{1,...,4}$ are given by $\Gamma_1 = \Gamma_4 = \gamma \cdot q$ and $\Gamma_2 = \Gamma_3 = \gamma \cdot (2q + p)$. Evaluation of Eq. (66) yields

$$\tilde{\Gamma}_4^{(2)}(0) = \tfrac{7}{2}\hat{e}^2 \gamma_0. \tag{67}$$

Hence, the second-order contribution to the vertex function becomes

$$\tilde{\Gamma}^{(2)}(0) = \tilde{\Gamma}_1^{(2)}(0) + \tilde{\Gamma}_2^{(2)}(0) + 2\tilde{\Gamma}_3^{(2)}(0) + 2\tilde{\Gamma}_4^{(2)}(0), \tag{68}$$

such that the dressed vertex function can be written as a series in $\hat{e}$:

$$\tilde{\Gamma}_0 = \tilde{e}\gamma_0 \approx \left(1 + \hat{e} + \tfrac{33}{2}\hat{e}^2 + O(\hat{e}^3)\right)\gamma_0. \tag{69}$$

This expression reproduces exactly the result which we have obtained for the dressed vertex function in Eq. (57). Therefore, we obtain from Eqs. (49), (69), and (57) for the modified conductivity

$$\tilde{\sigma} \approx (1 + O(\hat{e}^3))\sigma_0; \tag{70}$$

i.e., the leading correction is of the order g_0^6. However, we can show to every order in perturbative expansion that corrections arising from the propagator renormalization are exactly canceled by their counterparts departing from the electron-photon vertex renormalization. Consider the definition of the quasiparticle weight Z_0^{-1} given in Eq. (45). Since the lattice deformations are static, all propagators inside the diagram depend only on the external Matsubara frequency, which thus becomes an independent parameter. Hence the derivative with respect to the Matsubara frequency should be applied to every propagator. Taking such a derivative of an average free propagator

$$\langle G_0(q_0, q + k)\rangle_k = \int_k \frac{q_0 \gamma_0 + (q_\mu + k_\mu)\gamma_\mu}{q_0^2 + (q + k)^2}, \tag{71}$$

at zero external momentum and frequency we obtain

$$\frac{\partial}{\partial q_0}\langle G_0(q_0, q + k)\rangle_k|_{Q=0} = -\langle G_0(0, k)\gamma_0 G_0(0, k)\rangle_k. \tag{72}$$

Equation (72) suggests that the expressions under the integrals must be equal up to an irrelevant constant. Therefore, each derivative of the free propagator with respect to the external frequency generates upon sending external momenta and frequency to zero a bare electron-photon vertex. An irreducible nth-order diagram of the electronic self-energy contains $2n - 1$ electronic propagators. Therefore, by applying a derivative with respect to the frequency q_0 to such a diagram, $2n - 1$ irreducible corrections to the electron-photon interaction vertex are generated. This mimics term by term a perturbative

series for the dressed vertex. This can be seen very clearly if we look at the self-energy diagrams depicted in Fig. 7. Replacing electronic propagators successively by a bare electron-phonon interaction vertex and sending external momenta to zero, we reproduce exactly the vertex-correction diagrams shown in Fig. 9. We therefore can link each nth ($n \geqslant 1$) term in the perturbative series of self-energy to the corresponding vertex function correction:

$$\frac{\partial}{\partial q_0}\Sigma^{(n)}(Q)|_{Q=0} = -\tilde{\Gamma}_0^{(n)}(0,0,0). \tag{73}$$

Summing over all n and subtracting γ_0 on both sides, we then can assemble all contributions, arriving at

$$\frac{\partial}{\partial q_0}G^{-1}(Q)|_{Q=0} = \tilde{\Gamma}_0(0,0,0). \tag{74}$$

On the right-hand side we have the charge renormalization $\tilde{e}\gamma_0$ defined in Eq. (46), while the left-hand side represents the wave-function renormalization factor $Z_0^{-1}\gamma_0$ due to Eq. (44). Therefore, Eq. (74) postulates the equality

$$Z_0^{-1} = \tilde{e},$$

which leads to the exact result for the modified conductivity:

$$\tilde{\sigma} = \sigma_0. \tag{75}$$

Importantly, Eq. (74) is obtained without special emphasis on a disorder type and is not restricted to the considered type. The only requirement is that the corresponding term should not violate the chiral symmetry of the pure graphene Hamiltonian and it must be a quenched disorder.

VI. CONCLUSIONS

In the present paper we address the question of the effect that random deformations may have on the transport in graphene. The common belief is that surface corrugations in graphene influence its electronic transport properties, mainly the optical conductivity. It is possible to describe deformations in graphene by a gauge field that couples to the fermions living on the two-dimensional sheet. We performed perturbative calculations of the corrections due to lattice deformations to the optical conductivity. Our results contrast the suggestions made in Refs. 17 and 21, where a substantial effect of the defects on the conductivity is proposed. We have found that the minimal conductivity is robust with respect to the surface corrugations.

APPENDIX

Below be evaluate the irreducible polarization of clean graphene starting with Eq. (41). Upon performing the trace over the pseudospin space, we arrive at

$$\Pi(K) = 2 \int_P \frac{2p_0(p_0 + k_0) - P(P + K)}{P^2(P + K)^2},$$

where $PK = p_0 k_0 + \boldsymbol{p} \cdot \boldsymbol{k}$. Employing the Feynman parametrization

$$\frac{1}{AB} = \int_0^1 \frac{dx}{[xA + (1 - x)B]^2},$$

and shifting $P \rightarrow P - xK$, we symmetrize the denominator with respect to P. Therefore, odd powers of P appearing in the numerator may be dropped. We arrive at

$$\Pi(K) = 2 \int_P \int_0^1 dx \frac{2p_0^2 - P^2 + x(1 - x)[K^2 - 2k_0^2]}{[P^2 + x(1 - x)K^2]^2}.$$

Exploiting the rotational invariance, we replace $p_0^2 = P^2/3$ and use formulas of dimensional regularization:

$$\int \frac{d^d k}{(2\pi)^d} \frac{1}{(k^2 + \Delta)^n} = \frac{1}{(4\pi)^{d/2}} \frac{\Gamma\left(n - \frac{d}{2}\right)}{\Gamma(n)\Delta^{n-d/2}},$$

$$\int \frac{d^d k}{(2\pi)^d} \frac{k^2}{(k^2 + \Delta)^n} = \frac{1}{(4\pi)^{d/2}} \frac{d}{2} \frac{\Gamma\left(n - \frac{d}{2} - 1\right)}{\Gamma(n)\Delta^{n-d/2-1}},$$

which yields, after integrating out x, the result of Eq. (42).

[1] K. S. Novoselov, A. K. Geim, S. V. Morozov, D. Jiang, M. I. Katsnelson, I. V. Grigorieva, S. V. Dubonos, and A. A. Firsov, Nature (London) **438**, 197 (2005).

[2] K. S. Novoselov, E. McCann, S. V. Morozov, V. I. Fal'ko, M. I. Katsnelson, U. Zeitler, D. Jiang, F. Schedin, and A. K. Geim, Nat. Phys. **2**, 177 (2006).

[3] M. I. Katsnelson, K. S. Novoselov, and A. K. Geim, Nat. Phys. **2**, 620 (2006).

[4] Y. Zhang, Y.-W. Tan, H. L. Stormer, and P. Kim, Nature (London) **438**, 201 (2005).

[5] E. Fradkin, Phys. Rev. B **33**, 3263 (1986).

[6] P. A. Lee, Phys. Rev. Lett. **71**, 1887 (1993).

[7] A. W. W. Ludwig, M. P. A. Fisher, R. Shankar, and G. Grinstein, Phys. Rev. B **50**, 7526 (1994).

[8] K. Ziegler, Phys. Rev. B **55**, 10661 (1997); Phys. Rev. Lett. **80**, 3113 (1998).

[9] E. G. Mishchenko, Phys. Rev. Lett. **98**, 216801 (2007); Europhys. Lett. **83**, 17005 (2008).

[10] D. E. Sheehy and J. Schmalian, Phys. Rev. Lett. **99**, 226803 (2007).

[11] I. F. Herbut, V. Juričić, and O. Vafek, Phys. Rev. Lett. **100**, 046403 (2008).

[12] F. de Juan, A. G. Grushin, and M. A. H. Vozmediano, Phys. Rev. B **82**, 125409 (2010).

[13] K. Ziegler, Phys. Rev. B **75**, 233407 (2007).

[14] M. Ishigami, J. H. Chen, W. G. Cullen, M. S. Fuhrer, and E. D. Williams, Nano Lett. **7**, 1643 (2007).

[15] J. C. Meyer, A. K. Geim, M. I. Katsnelson, K. S. Novoselov, T. J. Booth, and S. Roth, Nature (London) **446**, 60 (2007).

[16] E. Stolyarova, K. T. Rim, S. Ryu, J. Maultzsch, P. Kim, L. E. Brus, T. F. Heinz, M. S. Hybertsen, and G. W. Flynn, Proc. Natl. Acad. Sci. USA **104**, 9202 (2007).

[17] A. Cortijo and M. A. H. Vozmediano, Phys. Rev. B **79**, 184205 (2009).

[18] D. V. Khveshchenko, Europhys. Lett. **82**, 57008 (2008).

[19] K. Ziegler, Phys. Rev. Lett. **102**, 126802 (2009); Phys. Rev. B **79**, 195424 (2009); J. H. Bardarson, M. V. Medvedyeva, J. Tworzydlo, A. R. Akhmerov, and C. W. J. Beenakker, *ibid.* **81**, 121414(R) (2010); K. Ziegler and A. Sinner, *ibid.* **81**, 241404(R) (2010).

[20] A random vector potential has a strong effect on the local density of states fluctuations, leading to long-range correlations; see K. Ziegler, Phys. Rev. B **78**, 125401 (2008).

[21] M. A. H. Vozmediano, M. I. Katsnelson, and F. Guinea, Phys. Rep. **496**, 109 (2010).

[22] A. R. Kavalov, I. K. Kostov, and A. G. Sedrakyan, Phys. Lett. B **175**, 331 (1986).

[23] A. Cortijo and M. A. H. Vozmediano, Europhys. Lett. **77**, 47002 (2007).

[24] A. Cortijo and M. A. H. Vozmediano, Nucl. Phys. B **763**, 293 (2007).

[25] F. de Juan, A. Cortijo, and M. A. H. Vozmediano, Phys. Rev. B **76**, 165409 (2007).

[26] G. W. Semenoff, Phys. Rev. Lett. **53**, 2449 (1984).

[27] A. Sedrakyan and R. Stora, Phys. Lett. B **188**, 442 (1987).

[28] B. A. Dubrovin, A. T. Fomenko, and S. P. Novikov, *Modern Geometry—Methods and Applications* (Springer, New York, 1984), Pt. 1.